HHS Public Access

Author manuscript

ACS Appl Mater Interfaces. Author manuscript; available in PMC 2024 July 10.

Published in final edited form as:

ACS Appl Mater Interfaces. 2021 November 10; 13(44): 52321–52332. doi:10.1021/acsami.1c14506.

Nanoparticle-Enabled Multiplexed Electrochemical Immunoassay for Detection of Surface Proteins on Extracellular Vesicles

Seonhwa Lee,
Department of Physiology and Biomedical Engineering, Mayo Clinic, Rochester, Minesotta 55905, United States

Bruno P. Crulhas,
Department of Physiology and Biomedical Engineering, Mayo Clinic, Rochester, Minesotta 55905, United States

Sonja Suvakov,
Division of Nephrology and Hypertension, Mayo Clinic, Rochester, Minesotta 55905, United States

Stanislav V. Verkhoturov,
Department of Chemistry, Texas A&M University, College Station, Texas 77843, United States

Dmitriy S. Verkhoturov,
Department of Chemistry, Texas A&M University, College Station, Texas 77843, United States

Michael J. Eller,
Department of Chemistry and Biochemistry, California State University Northridge, Northridge, California 91330, United States

Harmeet Malhi,
Division of Gastroenterology and Hepatology, Mayo Clinic, Rochester, Minesotta 55905, United States

Vesna D. Garovic,
Division of Nephrology and Hypertension, Mayo Clinic, Rochester, Minesotta 55905, United States

Emile A. Schweikert,
Department of Chemistry, Texas A&M University, College Station, Texas 77843, United States

Corresponding Author Alexander Revzin – *Department of Physiology and Biomedical Engineering, Mayo Clinic, Rochester, Minesotta 55905*, United States; Revzin.Alexander@mayo.edu.

Author Contributions

S.L., B.P.C., S.S., S.V.V., and D.S.V. performed the experiments; S.L., M.J.E., H.M., V.D.G., E.A.S., G.S., and A.R. analyzed the data; S.L. and A.R. wrote the article with input from all authors. All authors have given approval to the final version of the article.

ASSOCIATED CONTENT

Supporting Information

The Supporting Information is available free of charge at https://pubs.acs.org/doi/10.1021/acsami.1c14506.

UV–vis spectra, TEM images, EDX spectra, MS spectra, and SWV of immunoprobes; electrochemical experiment setup; NTA analysis and SEM images of urinary EVs; optimization of experimental parameters; detection of nephrin and podocin; flow cytometry analysis of urine samples; and comparison of analytical performance of various immunosensors for EVs (PDF)

Complete contact information is available at: https://pubs.acs.org/10.1021/acsami.1c14506

The authors declare no competing financial interest.

Gulnaz Stybayeva,
Department of Physiology and Biomedical Engineering, Mayo Clinic, Rochester, Minesotta 55905, United States; Sersense Inc., Rochester, Minesotta 55905, United States

Alexander Revzin
Department of Physiology and Biomedical Engineering, Mayo Clinic, Rochester, Minesotta 55905, United States

Abstract

Extracellular vesicles (EVs) are lipid bilayer particles secreted from various cells. EVs carry molecular information of parent cells and hold considerable promise for early disease diagnostics. This paper describes a general strategy for multiplexed immunosensing of EV surface proteins, focusing on surface markers CD63, CD81, nephrin, and podocin to prove the concept. This sensing strategy entailed functionalizing gold nanoparticles (AuNPs) with two types of antibodies and then tagging with metal ions, either Pb^{2+} or Cu^{2+}. The metal ions served as redox reporters, generating unique redox peaks at −0.23 and 0.28 V (vs Ag/AgCl) during electrochemical oxidation of Pb^{2+} and Cu^{2+}, respectively. Capture of EVs on the working electrode, followed by labeling with immunoprobes and square wave voltammetry, produced redox currents proportional to concentrations of EVs and levels of expression of EV surface markers. Importantly, metal-ion tagging of immunoprobes enabled detection of two EV surface markers simultaneously from the same electrode. We demonstrated dual detection of either CD63/CD81 or podocin/nephrin surface markers from urinary EVs. The NP-enabled immunoassay had a sensitivity of 2.46×10^5 particles/mL (or 40.3 pg/mL) for CD63- and 5.80×10^5 particles/mL (or 47.7 pg/mL) for CD81-expressing EVs and a linear range of four orders of magnitude. The limit of detection for podocin and nephrin was 3.1 and 3.8 pg/mL, respectively. In the future, the capacity for multiplexing may be increased by extending the repertoire of metal ions used for redox tagging of AuNPs.

Graphical Abstract

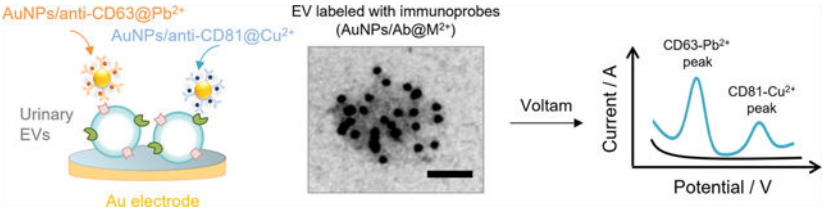

Keywords

extracellular vesicles; immunoassays; electrochemical biosensors; simultaneous detection; biomarker

INTRODUCTION

Extracellular vesicles (EVs) are membrane-bound phospholipid nanovesicles secreted by cells and present in various body fluids, such as serum, urine, and saliva.[1–3] Based on

their biogenesis, EVs are categorized into exosomes (formed as intraluminal vesicles within multivesicular bodies) and microvesicles (formed by the regulated release or outward budding of the plasma membrane).[4–6] Several transmembrane proteins, such as tetraspanins (CD9, CD63, CD81, and CD82), integrins, and heat shock proteins are ubiquitous to EVs.[5,6] Given that CD63 and CD81 are present on 60 to 80% of urinary EVs,[7] these markers were chosen for sensor development and validation described in this study.

EVs appear in circulation while carrying markers specific to a distant disease site and, therefore, hold promise for early diagnosis of diseases ranging from cancer to preeclampsia and non-alcoholic steatohepatitis.[8–10] Urinary EVs are particularly well-suited for diagnosis of renal diseases.[11,12] For example, members of our team have shown that the levels and ratios of EV surface markers podocin and nephrin correlate with preeclampsia—a renal disease associated with significant pregnancy complications.[9,13] In the process of analyzing clinical samples, we found that relative or ratiometric quantification of EV surface markers accounted for patient-to-patient variability in surface marker expression and was preferred to measurements of single surface markers. Therefore, the ability to detect multiple surface markers from the same population of EVs was a key design parameter for our detection strategy.

Given their potential for early disease diagnosis and longitudinal follow up of patients, there is a strong interest in developing novel strategies for isolation and detection of EVs. We note that the focus of this paper is on establishing EV detection methodology and direct the reader to excellent comprehensive reviews on the topic of EV isolation.[14,15] Although a number of exciting optical/plasmonic and electrochemical biosensing strategies for detection of EV biosensing have been reported in the literature,[16–24] there remains a need for multiplexed, simple, and sensitive means of quantifying EV surface markers. An excellent recent example of plasmonic EV detection was published by Fan et al.[16] who employed surface plasmon resonance (SPR) imaging to capture exosomes on an antibody (Ab)-modified sensing chip and detected three exosomal surface markers expressing CD63, EpCAM, and EGFR. Despite the fact that Ab-modified gold nanoparticles (AuNPs) were used to amplify SPR signals from bound exosomes, the limit of detection (LOD) reported for this study was in the 10^7 particles/mL range. This is two orders of magnitude higher than the LOD for our NP-enabled immunoassay. Another excellent plasmonic approach was reported by Liang, Hu, and co-workers who captured EVs and then used Ab-functionalized nanorods and nanospheres for detecting two surface markers on the same population of EVs.[17] Although possessing multiple advantages including minimal volume and sample prep requirements, the LOD for this nanoplasmonic strategy was 0.2 ng/μL, which was not nearly as sensitive as the 40 pg/mL detection limit achieved with our detection approach.

Electrochemical biosensors are used extensively in medicine, typically in a point-of-care setting where rapid, simple, and inexpensive means of detecting analytes are important.[25,26] There are a number of publications describing the use of electrochemical sensing for detection of EVs.[10,19–24,27] For example, Boriachek et al. reported an electrochemical immunosensor for detection of tumor-specific EVs using streptavidin-coated CdSe quantum dots functionalized with biotinylated Abs against HER-2 and FAM134B.[19] After capture of EVs, quantum dots were dissolved with acid and metal ions were concentrated on the

electrode surface using anodic stripping voltammetry and measured using square wave voltammetry (SWV). This method had an excellent detection limit of 10^5 EV particles/mL; however, no multiplexing was demonstrated. In another example of electrochemical detection of EVs, Lee and colleagues developed a microtiter plate-like platform first in eight wells and most recently in a 96-well format with each well serving as an electrochemical cell.[23] EVs were first captured on magnetic beads inside the wells, washed, and then labeled with secondary Abs carrying *horseradish peroxidase* (HRP). Although providing an exceptional example of an electrochemical platform for high-throughput testing of EV surface markers, this strategy afforded a LOD of 10^7 EV particles/mL (compared to 10^5 particles/mL reported here). Furthermore, reliance on the HRP/tetramethylbenzidine enzymatic amplification reaction for the electrochemical signal likely necessitated precise control over timing of measurements and may have contributed to a complicated platform design where each well was addressed by its own potentiostat, and all measurements were made in parallel.[20,23]

In contrast to the strategy described above, the electrochemical EV detection approach developed by us has an excellent detection limit without the need for amplification, with the signal remaining stable over the course of days. This approach (outlined in Scheme 1) involved capturing EVs on a working electrode, washing unbound EVs, and then labeling with electroactive immunoprobes that targeted either tetraspanins, CD63, and CD81, or renal markers podocin and nephrin. Surface marker expression was analyzed by SWV. The design of immunoprobes for EV analysis represented the key innovation of this sensing strategy. Immunoprobes consisted of AuNPs functionalized with Abs and doped with metal ions such that a surface marker (e.g., CD63 or CD81) was paired with a metal-ion type (either Pb^{2+} or Cu^{2+}). This allowed us to quantify both surface markers from the same population of EVs captured on the same electrode. Our NP-enabled immunoassay had excellent figures of merit: detection limit of 10^5 particles/mL with linear range extending to 10^8 particles/mL. We estimate that each immunoprobe contained 10^4 metal ions, which explains the excellent detection limit without the need for amplification steps. Given a wide repertoire of metal ions available for redox labeling (e.g., Zn^{2+}, Cd^{2+}, Ag^{+}, and Fe^{3+}),[28–30] we envision further expanding the capacity for multiplexing and plan to apply this NP-enabled immunoassay for analysis of clinical samples in the future.

RESULTS AND DISCUSSION

Characterization of AuNPs/Abs@M^{2+} Immunoprobes.

We produced two populations of immunoprobes: AuNPs/anti-CD63@Pb^{2+} and AuNPs/anti-CD81@Cu^{2+}. As shown in Figure 1A, Ab molecules were covalently bound to *N*-hydroxysuccinimide (NHS)-activated AuNPs using 1-ethyl-3-(3-dimethylaminopropyl)carbodiimide (EDC)–NHS chemistry.[31] Immobilized Abs provided amine-rich groups which served as anchoring sites for absorption of Pb^{2+} and Cu^{2+}. Metal ion–protein interactions have been reported extensively in the literature and are hypothesized to occur via inorganic coordination bonding between the metal ions and amines.[32–34]

Several analytical approaches were used to characterize assembly and composition of immunoprobes. Ultraviolet–visible spectroscopy (UV–vis) provided a simple means of

monitoring functionalization of AuNPs with Abs. Binding of Abs led to a redshift of AuNPs from 522 to 525 nm and was associated with the appearance of a characteristic protein peak at 280 nm (see Figure S1). Incorporation of metal ions resulted in further redshift of AuNPs —a behavior that has been reported previously.[35,36] To further demonstrate the attachment of metal ions to the immunoprobes, energy-dispersive X-ray analysis (EDX) characterization was employed (see Figure S2). The EDX spectra for the AuNPs/anti-CD63@Pb^{2+} and AuNPs/anti-CD81@Cu^{2+} again indicate that these nanocomposites comprise Au and Pb (or Cu) elements. Although useful for confirming modification of AuNPs, UV–vis and EDX cannot be used to confirm the co-localization of Abs and metal ions on the same AuNP.

To test for co-localization, we used nanoprojectile secondary-ion mass spectrometry (NP-SIMS). NP-SIMS involves bombarding the surface with a suite of individual nanoprojectiles (e.g., Au_{400}^{4+}) separated in time and space, allowing for mass spectrometry measurements on the nanoscale.[37] In our study, NP-SIMS was used to examine immunoprobes for co-localization of metal ions and Abs on the AuNPs. Samples for NP-SIMS analysis were prepared on a clean silicon substrate using the Marangoni flow-assisted method which, resulted in a sparse distribution of NPs.[38] NP-SIMS was then used to analyze three types of samples; AuNPs/anti-CD63@Pb^{2+}, AuNPs/anti-CD81@Cu^{2+}, and a negative control containing AuNPs/anti-CD63 without metal ions (see Figure S3). Measurements on AuNPs were identified and selected based on the detection of gold clusters (e.g., Au_2^+ or Au_3^+). The successful assembly of immunoprobes was evaluated by examining the co-emitted secondary-ion characteristics of the Abs and metal ions. Figure 1B shows the mass spectra from NP-SIMS analysis of AuNPs/anti-CD63@Pb^{2+} and AuNPs/anti-CD81@Cu^{2+} immunoprobes. Both mass spectra contained an organic fragment, $(CH_3NH)_2CH^+$, attributed to Abs, co-emitted with Au ions originating from AuNPs. This pointed to successful immobilization of Abs on AuNPs. Additionally, in the same set of measurements, we observed the co-emission of characteristic metal-ion peaks for Pb^+ ($^{206}Pb^+$, $^{207}Pb^+$, and $^{208}Pb^+$) and Cu^+ ($^{63}Cu^+$ and $^{65}Cu^+$). These observations demonstrate that Abs and metal ions were co-localized in close proximity (within 10 nm) on the surface of individual AuNPs.

Additional characterization of immunoprobes was carried out by transmission electron microscopy (TEM). Imaging of AuNPs/anti-CD63, AuNPs/anti-CD63@Pb^{2+}, and AuNPs/anti-CD81@Cu^{2+} revealed that all three NP types were of similar size, with a mean diameter of ~18 nm (see Figure S2). This observation suggested that our preparation protocol produced similar-sized immunoprobes for detection of CD63 and CD81 and that incorporation of metal ions did not affect morphology or size of NPs.

In summary, multiple surface analysis techniques were used to confirm the presence of ~18 nm AuNPs containing either anti-CD63@Pb^{2+} or anti-CD81@Cu^{2+} complexes.

Assessing Redox Activity and Stability of AuNPs/Abs@M^{2+}.

Before proceeding to EV detection, we took several steps to characterize and optimize the AuNPs/Abs@M^{2+} immunoprobes. At the first stage of characterization, immunoprobes were immobilized on Au electrodes using a Nafion membrane.[39,40] The redox peaks of AuNPs/anti-CD63@Pb^{2+} and AuNPs/anti-CD81@Cu^{2+} were then examined by SWV in 0.2

M HAc/NaAc at pH 4.5. All electrochemical characterization experiments described in this paper were carried out in a custom-built three-electrode electrochemical cell (see Figure S4) with Ag/AgCl reference and Pt counter electrodes. Pieces of silicon wafers (12 by 12 mm^2) with a 100 nm layer of sputtered Au were used as working electrodes.

The two types of immunoprobes were analyzed by SWV either individually or as a mixture. As shown in Figure 2A, distinct redox peaks of Pb^{2+} and Cu^{2+} were observed in the presence of AuNPs/anti-CD63@Pb^{2+} (curve a) or AuNPs/anti-CD81@Cu^{2+} (curve b). Next, we immobilized the two-tag mixture on Au electrodes and performed SWV. Figure 2A (curve c) demonstrates the presence of two distinct redox peaks at −0.23 and 0.28 V (vs Ag/AgCl), corresponding to electrochemical oxidation of Pb^{2+} and Cu^{2+} from AuNPs/anti-CD63@Pb^{2+} and AuNPs/anti-CD81@Cu^{2+}, respectively, which is similar to previous reports about the redox peak potential of Pb^{2+} and Cu^{2+} based on the Au substrate.[41–44] Moreover, a similar amplitude of peak current was observed for individual populations or a mixed population of immunoprobes. This indicated that AuNPs/anti-CD63@Pb^{2+} and AuNPs/anti-CD81@Cu^{2+} may be used concurrently on the same electrode. Additionally, the amplitude of two redox peaks was proportional to the concentration of each NP population (curve d). Later in this paper, we will demonstrate that differences in the levels of surface marker expression may be related to the amplitude of redox peaks.

As the next stage in immunoprobe characterization, we evaluated the stability of the metal ion incorporation into NPs. For these experiments, immunoprobes were stored at 4 °C in a 4-(2-hydroxyethyl)piperazine-1-ethanesulfonic acid (HEPES) solution for 8 days and were tested daily using the electrochemistry approach described above. As seen from Figure 2B, only minimal decline in redox activity (5 to 8%) was observed for AuNPs/anti-CD63@Pb^{2+} and AuNPs/anti-CD81@Cu^{2+} over the course of 8 days, suggesting that metal ions remained stably incorporated into immunoprobes during storage.

Labeling EVs with Immunoprobes.

Urinary EVs were characterized by NP tracking analysis (NTA) and TEM. NTA analysis revealed the bimodal distribution of EVs sizes, with 60% of particles having a diameter of 100 ± 45 nm, dimensions typical of small EVs, and 40% of particles with a diameter of 220 ± 75 nm, typical of large EVs (Figure S5). The concentration of EVs in a typical undiluted urine sample was 1.14×10^8 particles/mL. TEM images revealed that particles isolated from urine were of spherical shape with a lipid bilayer membrane—morphology typical of EVs (Figure 3A).[45]

After confirming successful isolation of EVs, we proceeded to label EVs with immunoprobes. For this experiment, a sample of isolated EVs (1.14×10^8 particles/mL) was incubated with AuNPs/anti-CD63@Pb^{2+} (2 nM) at room temperature for 6 h before TEM measurement. As seen from a representative TEM image in Figure 3B, AuNPs/anti-CD63@Pb^{2+} immunoprobes were bound to EVs, suggesting affinity for the surface marker CD63.

Characterization of NP-Enabled Electrochemical Immunoassay.

To characterize electrochemical immunoassay, EVs were captured on poly-L-lysine (PLL)-coated Au electrodes and then labeled with immunoprobes. There are several options for creating surfaces with affinity to EVs (e.g., Abs for Annexin V). In the present study, we chose to work with PLL surfaces due to the simplicity of EV capture based on electrostatic interactions, presence of primary amines for immobilization of proteins, and a high electroactive surface area.[46,47]

The process of electrode modification is shown in Figure 3C. Here, Au electrodes were first incubated with 11-mercaptoundecanoic acid (MUA) to form a self-assembled monolayer (SAM) and then were functionalized with PLL using EDC–NHS coupling chemistry. The electrodes were then incubated with EVs that were captured via electrostatic interactions and finally were coated with bovine serum albumin (BSA) to prevent nonspecific binding. Finally, EV-containing surfaces were incubated with immunoprobes, AuNPs/anti-CD63@Pb^{2+} and AuNPs/anti-CD81@Cu^{2+}.

Electrical impedance spectroscopy (EIS) with 5 mM $[Fe(CN)_6]^{4-/3-}$ in 0.1 M KCl was used to confirm individual steps of the electrode modification workflow. Impedance measurements made after individual surface modification steps are summarized in Figure 3D. The bare Au electrode exhibited a small semicircle at high frequencies with an R_{ct} of 25 Ω (curve a). After SAM formation with MUA, the R_{ct} increased to 4114 Ω (curve b) due to the presence of the COOH terminal group and the carbon chain of the SAM, which hinder diffusion and electron transport for the negatively charged $[Fe(CN)_6]^{4-/3-}$ redox couple.[48,49] Subsequent treatment of the SAM-modified electrode with EDC–NHS resulted in a lower value for R_{ct} (2010 Ω) (curve c), demonstrating that the $-COO^-$ groups of SAM were successfully functionalized with EDC–NHS. After assembly of PLL (curve d), the value for R_{ct} decreased further to 1497 Ω due to the abundance of positively charged amino groups providing electrostatic attraction force for $[Fe(CN)_6]^{4-/3-}$. After incubation with EVs (curve e), the R_{ct} value increased to 2766 Ω likely due to increased resistance and presences of negative charges on the EV surfaces. Immobilization of BSA increased the resistance of the electrode and led to an increase in the R_{ct} value to 3521 Ω (curve f). Incubation of the substrate with AuNPs/anti-CD63@Pb^{2+} caused the R_{ct} to drop to 1814 Ω (curve g), suggesting that AuNPs/anti-CD63@Pb^{2+} promoted electron transfer. Overall, EIS confirmed assembly of sensing surfaces, capture of EVs, and attachment of immunoprobes.

Optimizing Performance of Electrochemical Immunoassay.

We explored and optimized parameters deemed likely to improve performance of the immunoassay including EV incubation time, immunoprobe labeling time, and pH of the electrolyte solution. Redox activity was assessed by SWV after incubating the PLL-coated Au electrodes with 1.14×10^8 EV particles/mL and then labeling with AuNPs/anti-CD63@Pb^{2+} and AuNPs/anti-CD81@Cu^{2+} immunoprobes. Previous reports have shown that pH of the electrolyte solution may affect the electrochemical behavior of metal ions incorporated into NPs.[28–30] Therefore, we analyzed performance of the NP-enabled immunoassay for the electrolyte pH ranging from 3.5 to 6. As shown in Figure S6A, the

peak currents were obtained for pH 4.5, which was then chosen as operating pH for our detection experiments. A plausible explanation is that metal ions complexed with hydroxide ions and became inactive at a pH above 4.5.

The electrochemical signal was also a function of EV capture time, with the signal reaching a plateau at 180 min (Figure S6B). We note that the capture time was affected by the large volume of batch-mode electrochemical cells. The capture time will be decreased in the future by using a microfluidic flow-through electrochemical cell. The time of EV labeling with immunoprobes (AuNPs/Abs@M^{2+}) also affected the electrochemical signal, with 90% of the maximum signal being achieved after 60 min of incubation (Figure S6C).

Based on these optimization efforts, the following experimental conditions were maintained for all subsequent measurements: pH 4.5 for HAc/NaAc electrolyte, 120 min for incubation of the EV sample with the electrode, and 60 min for labeling the captured EVs with immunoprobes (AuNPs/Abs@M^{2+}).

Detecting Two EV Surface Markers from the Same Electrode and Assessing Cross-Reactivity of Immunoprobes.

Given our goal of multiplexed detection of EV surface markers, we wanted to ensure that the two types of immunoprobes developed in this study were not cross-reactive. To assess cross-reactivity, we prepared several Au electrodes with captured EVs and incubated these electrodes with AuNPs/anti-CD63@Pb^{2+} or AuNPs/anti-CD81@Cu^{2+} individually or as an equimolar mixture. As shown in Figure 3E, labeling with AuNPs/anti-CD63@Pb^{2+} produced a distinct Pb^{2+} redox peak at −0.23 V, which corresponded to CD63 expression levels (curve a). Similarly, labeling of EVs with AuNPs/anti-CD81@Cu^{2+} followed by SWV produced a redox peak at 0.28 V associated with oxidation of Cu^{2+} (curve b). When EV-containing electrodes were incubated with an equimolar mixture of AuNPs/anti-CD63@Pb^{2+} and AuNPs/anti-CD81@Cu^{2+}, two distinct redox peaks were generated from the same electrode (curve c). As one way of confirming specificity of the measurement, the electrode surface without EVs was exposed to immunoprobes and then washed. As seen from Figure 3E (curve d), no SWV signal was observed at −0.23 or 0.28 V redox potentials for Pb^{2+} and Cu^{2+}, respectively, suggesting that generation of an electrochemical signal from immunoprobes depended on the presence of EVs.

The amplitude of peak currents associated with CD63 and CD81 expression was nearly identical for single-plex or dualplex detection, suggesting that (1) steric hindrance did not affect detection of individual surface markers and (2) there was no cross-reactivity between the two types of immunoprobes. Thus, results presented in Figure 3E confirmed that our strategy could be used to detect two EV surface markers from the same electrode.

Sensitivity and Specificity of the NP-Enabled Electrochemical Immunoassay.

As the next characterization step, we assessed figures of merit for this immunoassay: detection limit and dynamic range. Au electrodes were functionalized with different concentrations of EVs, then labeled with a mixed population of two immunoprobes, and finally analyzed by SWV. Scanning electron microscopy (SEM) analysis (see Figure S7) was used to confirm preparation of substrates with varying surface densities of EVs. As depicted

in Figure 4A, amplitude of oxidation peaks for Pb^{2+} and Cu^{2+}, corresponding to CD63 and CD81, respectively, increased as EV concentration was varied from 1.14×10^6 to 1.14×10^8 particles/mL. For comparison, only negligible redox activity (Figure 4A, dashed line) was observed when the substrate containing high surface density of EVs (10^8 particles/mL) was exposed to immunoprobes carrying isotype control (IgG) Abs (i.e., AuNPs/IgG@Pb^{2+} and AuNPs/IgG@Cu^{2+}). These results confirmed that redox peaks associated with CD63 and CD81 were a function of EV surface density and that electrochemical activity was associated with specific Ag–Ab interactions. Because the amplitude and shape of redox peaks may be affected by factors other than electron transfer (e.g., solution resistance and electrode preparation), we sought a more objective electrochemical parameter associated with EV signals. This was achieved by integrating the area under the redox peak to obtain the total amount of charge (Q) associated with each EV concentration (see Figure 4B). Then, Q values were normalized according to the formula (normalized Q, $\overline{Q} = Q_{\text{EVs}} - Q_{\text{isotype control Abs}}$) and used to construct calibration curves. As seen from Figure 4C, a linear relationship was observed between normalized $\overline{Q}$ and the logarithm of the EV concentrations from 1.14×10^6 to 1.14×10^8 particles/mL for both CD63 and CD81. The LOD was calculated to be 2.46×10^5 particles/mL for CD63 and 5.80×10^5 particles/mL for CD81 with good reproducibility (RSD < 7.6% for $n = 5$). These detection limits were considerably lower than those of commercial/standard approaches: ELISA for CD63 and CD81 (e.g., an ELISA kit from System Biosciences reports a LOD of 5.2×10^9 and 8.34×10^9 particles/mL for CD63 and CD81, respectively),[50,51] western blot (10^{11}–10^{12} particles/mL), NTA (10^7–10^9 particles/mL), and flow cytometry (10^7–10^9 particles/mL).[51–55] To better evaluate how our detection approach compares to EV detection strategies being developed in academia, we tabulated LODs, dynamic range, and other assay characteristics from several recently published EV sensing strategies in Table S1.[10,18–22,56–59] Comparison with previously published sensing strategies reveals that our approach has an excellent detection limit, requires a minimal number of steps to generate signals, uses simple instrumentation, and, importantly, is amenable to multiplexing.

In addition to quantifying numbers of EVs, our strategy may also provide concentrations of the surface markers. To assess protein-level detection limits for our electrochemical immunoassay, we immobilized different concentrations of recombinant CD63 and CD81 on MUA-functionalized electrodes using EDC–NHC chemistry. The electrodes containing various amounts of surface markers were then incubated with immunoprobes, washed, and analyzed using SWV. As shown in Figure 5A, calibration curves for CD63 and CD81 had a linear range of four logs from 0.05 to 500 ng/mL with a LOD of 37.3 pg/mL for CD63 and 41.1 pg/mL for CD81. After correlating the concentration of EVs to the concentration of protein (Figure 5B), the LOD corresponds to 40.3 pg/mL of CD63 (2.46×10^5 particles/mL) and 47.7 pg/mL of CD81 (5.80×10^5 particles/mL) of isolated EVs.

We wanted to further explore and explain the sensitivity of our electrochemical immunoassay. In the first set of experiments, we assessed the electrochemical signal as a function of immunoprobe concentration by challenging the PLL-functionalized Au electrodes (without EVs) with various concentrations of NPs (see Figure S8A). The lowest detectable signals were observed for 8.95×10^5 AuNPs/mL for both AuNPs/

anti-CD63@Pb^{2+} and AuNPs/anti-CD63@Cu^{2+} immunoprobes. Taking into account the dimensions of the electrochemical cell (120 μL volume and 0.5 cm^2 area) and assuming that all immunoprobes deposited on or interacted with the electrode surface, we estimate that a detectable SWV signal was achieved with as few as 2.2×10^5 AuNPs/cm^2 (or 2.2×10^{-3} AuNPs/μm^2). Combining calibration data from Figures 4 and S8A, we established a relationship between AuNPs and EVs (see Figure S8B) and estimated the number of AuNPs per EV to be ~10 for CD63 and ~1 for CD81 detection. This estimate is in agreement with TEM imaging of EVs labeled with CD63-targeting immunoprobes (see Figure 3B).

We hypothesized that one reason for low detection limits achieved with NP-enabled immunoassay is due to high electrochemical activity of AuNPs doped with metal ions and wanted to estimate metal-ion loading capacity of AuNPs. To estimate metal-ion loading, a known concentration of AuNPs doped with either Cu or Pb ions was injected into an electrochemical cell and analyzed by SWV (see Figure S8A). The metal-ion concentration was then established by determining the total charge (Q) from voltammetry data for the $2e^-$ transfer process. Using this approach, we estimate that for AuNPs/anti-CD63@Pb^{2+} present in a solution at 8.95×10^9 particles/mL, there are 8.75×10^{13} Pb^{2+} ions/mL or 9.78×10^3 Pb^{2+} ions/AuNP. For AuNPs/anti-CD81@Cu^{2+} present at a concentration of 8.95×10^9 particles/mL, there is 9.06×10^{13} Cu^{2+} ions/mL or 1.01×10^4 Cu^{2+} ions/AuNP. It is of note that we assume that all NPs in the solution interact with the electrode surface and contribute to the redox signal. This may be an overestimation which would mean that values for metal-ion loading per NP may be higher than those reported above.

Benchmarking NP-Enabled Electrochemical Immunoassay against Flow Cytometry.

In the next set of experiments, we wanted to employ clinical samples and compare performance of our immunoassay against standard technology. As noted earlier, our team has a strong interest in preeclampsia—disease that manifests itself by hypertension and renal damage.[11,12] We previously demonstrated that EVs carrying renal proteins nephrin and podocin may represent biomarkers of preeclampsia.[9] Given the potential clinical relevance of these biomarkers, we constructed immunoprobes targeting nephrin and podocin (AuNPs/anti-nephrin@Pb^{2+} and AuNPs/anti-podocin@Cu^{2+}). As a first step in implementing our electrochemical immunoassay, we assessed figures of merit, LOD, and dynamic range for these proteins. The protocol used here was similar to that described for detection of recombinant CD63 and CD81 (see Figure 5). Electrodes were functionalized with MUA and then different concentrations of proteins were immobilized on the electrodes using EDC–NHS chemistry. Three electrodes were analyzed for each concentration of protein. Results in Figure S9 reveal that the electrochemical immunoassay had excellent sensitivity for nephrin and podocin with a LOD of ~3 pg/mL and dynamic range extending to 500 ng/mL.

As the next step, we proceeded with comparison of our method against a standard approach. Our team has made extensive use of flow cytometry for characterizing nephrin and podocin expression in urinary EVs;[9] therefore, we chose to determine the ratios of these two proteins using our electrochemical immunoassay and benchmark against the ratios obtained with flow cytometry. Urine samples from six pregnant women ($n = 6$) were used for this comparison study. Unlike earlier experiments described in Figure 4 where EVs were

captured on the PLL-modified electrodes and then labeled with immunoprobes targeting CD63 and CD81 markers, here we used electrodes modified with anti-CD63 to capture EVs and then labeled EVs with anti-nephrin and anti-podocin immunoprobes (see Figure 6A). Blocking with BSA and extensive washing after EV capture and immunoprobe incubation steps were used to minimize nonspecific interactions with the electrodes. Figure 6B shows dual redox signals obtained with a representative sample. One can note that amplitude of the Cu^{2+}/podocin peak is higher than that of the Pb^{2+}/nephrin peak. Total charge (area under the curve) was analyzed for each peak and the ratio of podocin to nephrin was determined to be 3.33 for this sample. The analysis was conducted in triplicate (three electrodes) for each clinical sample with a total of six urine samples being tested. We also carried out flow cytometry analysis of the same set of urine samples. Figure 6C shows results of a flow cytometry analysis of the same sample that was analyzed electrochemically in Figure 6B. Importantly, our flow cytometry approach relies on TruCount beads to measure out precise volume and on microbeads ranging in size from 0.2 to 2 μm in order to gate on particles consistent in size with EVs (0.2 to 1 μm). EVs are also stained with isotype control Abs conjugated to relevant fluorophores to establish the background signal (see Figure S10 for description of flow cytometry experiments). These steps help us ensure that flow cytometry analysis is quantitative and may be compared between samples. Figure 6C shows a flow scattergram that, together with microbead-based gating and isotype control analysis (see Figure S10), was used to determine the podocin-to-nephrin ratio for this particular urine sample to be 3.24. This is comparable to the ratio of 3.33 obtained with electrochemical immunoassay (see Figure 6B). All six urine samples were analyzed in a similar manner with the podocin-to-nephrin ratios calculated by each method plotted together in Figure 6D. These data reveal excellent correlation between the two methods ($R^2 = 0.9$) and suggest that our approach accurately reflects podocin and nephrin expression levels measured by standard technology (flow cytometry). The results presented in Figure 6 are highly encouraging and pave the way for future use of the NP-enabled electrochemical immunoassay as a diagnostic approach.

CONCLUSIONS

This paper describes the development of a multiplexed electrochemical immunoassay for detection of EV surface markers. The immunoassay relied on AuNPs functionalized with anti-CD63 or anti-CD81 Abs and doped with Pb^{2+} and Cu^{2+} to produce redox signals. These AuNPs or immunoprobes were used to simultaneously detect pairs of biomarkers either CD63/CD81 or podocin/nephrin on urinary EVs. The immunoassay had excellent sensitivity, with detection limits of 2.46×10^5 particles/mL (40.3 pg/mL) for CD63 and 5.80×10^5 particles/mL (47.7 pg/mL) for CD81 and a linear range extending to 1.14×10^8 particles/mL. The LOD for podocin and nephrin was 3.1 and 3.8 pg/mL, respectively. The benefits of this electrochemical immunoassay include (1) simplicity of measurement using electrochemical readouts, (2) enhanced sensitivity compared to conventional immunoassays, and (3) detection of multiple EV surface markers using a single electrode. In the future, the multiplexing capability of this EV sensing strategy may be increased by expanding the repertoire of metal ions used as redox reporters. We also envision integrating this electrochemical immunoassay in a more point-of-care compatible microfluidic format. Such

a system will have considerable utility for EV-based early diagnosis of diseases ranging from cancer to preeclampsia and steatohepatitis.

MATERIALS AND METHODS

Materials.

4-Morpholineethanesulfonic acid (MES), HEPES, NHS-activated AuNPs (20 nm), $Pb(NO_3)_2$, $Cu(NO_3)_2$, PLL, MUA, EDC, NHS, and Tween-20 were purchased from Sigma-Aldrich (St. Louis, MO). A total urine EV isolation kit was purchased from Invitrogen (Carlsbad, CA). Single-donor human pregnancy urine was purchased from Innovative Research (Novi, MI). Dulbecco's phosphate-buffered saline (PBS) was purchased from Corning (Corning, NY). Ethyl alcohol (EtOH) was purchased from Electron Microscopy Sciences (Hat eld, PA), while isopropyl alcohol (IPA) was purchased from Honeywell (Charlotte, NC). Mouse anti-human CD63 and CD81 Abs and the mouse IgG isotype control were purchased from BD Biosciences (San Jose, CA). Mouse anti-human nephrin Abs were purchased from Santa Cruz Biotechnology (Santa Cruz, CA). Mouse anti-human podocin Abs were generated in Dr. Garovic's laboratory, Mayo Clinic Rochester (Rochester, MN). Human recombinant CD63, CD81, and nephrin proteins were purchased from R&D Systems (Minneapolis, MN). Human recombinant podocin protein was purchased from BioVendor (Brno, Czech Republic).

Synthesis of the AuNPs/Abs@M^{2+} Immunoprobes.

NHS-activated AuNPs were used to construct immunoprobes. The AuNPs (3.58×10^{11} NPs/mL) were incubated for 2 h in 180 μL of PBS buffer containing 40 μg of Ab solution. Subsequently, 20 μL of quencher solution was used to block the unreacted NHS sites on AuNPs. To separate the AuNP/Ab conjugates, the mixture was centrifuged at 6000*g* and 4 °C for 30 min and washed three times with HEPES buffer (0.02 M and pH 7.0). Then, AuNP/Ab conjugates (AuNPs/anti-CD63) were dispersed in 1 mL of HEPES buffer (0.02 M and pH 7.0) with 0.025% Tween 20.

For incorporation of metal ions, 20 μL of 10 mM $Pb(NO_3)_2$ aqueous solution was added drop by drop to dispersion of AuNPs. The mixture was stirred vigorously overnight at room temperature. After centrifugation and washing three times with deionized–distilled (DI) water containing 0.025% Tween 20, immunoprobes (AuNPs/anti-CD63@Pb^{2+} and AuNPs/anti-nephrin@Pb^{2+}) were redispersed in 1 mL of HEPES buffer (0.02 M and pH 7.0) and stored at 4 °C until use. The AuNPs/anti-CD81@Cu^{2+} and AuNPs/anti-podocin@Cu^{2+} immunoprobes were prepared by the same procedure. For preparation of isotype control immunoprobes (AuNPs/IgG@Pb^{2+} and AuNPs/IgG@Cu^{2+}), mouse IgG Abs were conjugated with AuNPs in the manner identical to that described above for anti-CD63 Abs.

Physicochemical Characterization of AuNPs/Abs@M^{2+} Immunoprobes.

A custom-built NP-SIMS instrument utilizing a gold liquid metal-ion source was used for analysis of immunoprobes.[60] The instrument was operated in the event-by-event bombardment/detection mode, which involves impacting the surface with a sequence of

individual nanoprojectiles separated in times and sample. The impact of each projectile results in the emission of ions from a volume 10 nm in diameter and up to 10 nm in depth. For each impact, the co-emitted secondary ions are collected and mass analyzed with a reflectron time-of-flight mass spectrometer.[61] Mass spectrometry analysis of each sample was performed in the positive-ion mode using ~1×10^6 projectile impacts of 440 keV Au_{400}^{4+}. Thus, 1×10^6 individual mass spectra were collected for each sample. Selecting these individual mass spectra based on the detection of an ion of interest allows for elemental/molecular characterization of co-localized moieties. EDX analysis was performed in conjunction with TEM using an Oxford X-max detector (Oxford Instruments, Concord, MA) to determine the purity and chemical dispersion. UV–vis was performed by scanning their absorption spectrum in the range from 200 to 800 nm using a NanoDrop OneC (Thermo Fisher Scientific, Waltham, MA) to characterize their conjugation features. The morphologies of immunoprobes were investigated using a Technai12 transmission electron microscope (FEI, Hillsboro, OR) operating at 80 kV.

Preparation of EVs.

We employed two types of samples in this study: (1) commercial pregnancy urine was used for some the early assay characterization experiments, and (2) clinical urine samples from pregnant women were used for validation of our electrochemical immunoassay against standard EV analysis technology (flow cytometry).

1. EVs were isolated from human pregnancy urine (Innovative Research) using a total EV isolation kit (Invitrogen, Carlsbad, CA, USA). Briefly, frozen urine was thawed in a water bath at 37 °C for 5 min. The samples were centrifuged at 2000*g* for 30 min at 4 °C to remove debris. The supernatant was then mixed with the EV isolation reagent and incubated for 1 h at room temperature. Then, the sample was centrifuged at 10,000*g* for 1 h at 4 °C. After the supernatant was discarded without disturbing the sediment, the sample was centrifuged at 10,000*g* for another 5 min at 4 °C. Afterward, the sediment EVs were resuspended in PBS.
2. Urine samples were obtained from pregnant women at the Mayo Clinic according to the IRB protocol 2104–05. A total of six samples were collected and used in this study. The samples were stored at −80 °C until further use. The samples were thawed at 37 °C for 5 min and then centrifuged at 2000*g* to remove debris. We note that unlike commercial urine samples described in the preceding paragraph, clinical samples did not undergo additional processing beyond debris removal.

Both commercial and clinical urine samples were characterized by NTA (Nanosight NS300 Malvern Panalytical, Malvern, UK) to evaluate particle size and concentration. EV concentration was adjusted to 3.10×10^9 particles/mL for clinical samples and used throughout the study.

Characterization of EV/NP Constructs Using TEM and SEM.

The morphologies of the EVs and immunogold staining sample were characterized by TEM using JEOL 1400 (JEOL USA Inc. Peabody, MA) at 80 kV. For this experiment, a sample of isolated EVs (1.14×10^8 particles/mL) was incubated with AuNPs/anti-CD63@Pb^{2+} (2 nM) at room temperature for 6 h before TEM measurement. SEM was used to confirm the presence of EVs on the PLL-modified electrodes using a Hitachi S-4700 cold field emission scanning electron microscope (Hitachi High Technologies America, Inc., Schaumburg, IL). For SEM measurement, PLL-modified electrodes were incubated for 2 h with different concentrations of urinary EVs (from 1.14×10^6 to 1.14×10^8 particles/mL). Afterward, the electrodes were washed with DI water to remove unbound EVs and then dried under a N_2 atmosphere. Next, the EV captured surfaces were sputter-coated with gold-palladium (Au/Pd) for 30 s.

Functionalization of Electrodes for EV Capture.

In this work, we used two types of molecules to capture EVs on the working electrode: (1) positively charged PLL-functionalized electrodes were used for some of the initial assay characterization and (2) anti-CD63-modified electrodes were employed for analysis of clinical urine samples. Initial cleaning and functionalization steps were identical for both types of surfaces. Au electrodes were first cleaned by sonication in IPA for 30 min and then exposed to oxygen plasma for 5 min at 150 mW (YES-G500, Yield Engineering Systems, Freemont, CA, USA). Subsequently, electrodes were immersed in 10 mM MUA in ethanol for 12 h and then rinsed with ethanol and DI water to create a SAM layer (Au/MUA). For covalent conjugation, electrodes were placed in a solution composed of a 1:1 ratio of 200 mM EDC and 100 mM of NHS in 0.1 M MES for 1 h and then rinsed with DI water (Au/MUA/EDC–NHS).

For immobilization of PLL, electrodes were then exposed to 100 μg/mL PLL solution in 1× PBS for 1.5 h, which resulted in covalent immobilization of this polypeptide. The electrodes were subsequently washed with 1× PBS to remove any unbound PLL molecules. Au/MUA/EDC–NHS/PLL electrodes were stored at 4 °C until use for detection. Figure 3C represents the electrode modification steps.

For immobilization of Abs, Au electrodes were first functionalized with MUA and activated with EDC–NHS as described above. Subsequently, the electrodes were incubated in 50 μg/mL solution of anti-CD63 in 1× PBS for 1.5 h. After washing with 1× PBS to remove any unbound Abs, the Au electrode was incubated in 1% BSA for 1 h to minimize non-specific interactions. After washing with 1× PBS again, electrodes modified with anti-CD63 were stored at 4 °C before use.

Electrochemical Detection of EVs.

To characterize NP-enabled immunoassay, we used a potentiostat (Interface 1010E Potentiostat, Gamry Instruments, Warminster, PA) performing SWV in a three-electrode system with the Au working, Pt counter, and Ag/AgCl electrode (in 3 M KCl) as reference electrodes. The SWV was performed in acetic acid/sodium acetate buffer (HAc/NaAc; 0.2 M and pH 4.5) at overpotentials of −0.6 to 0.6 V (vs Ag/AgCl) and 25 mV amplitude and

15 Hz frequency. Home-made electrochemical cells consisting of polydimethylsiloxane well mounted on a Au-coated piece of silicon (see Figure S4) were used in these studies. Each electrochemical cell had a volume of 120 μL and an effective electrode area of 0.5 cm^2.

PLL-modified electrodes were used for detection of CD63 and CD81. These electrodes were incubated for 2 h with different concentrations of urinary EVs (from 1.14×10^6 to 1.14×10^8 particles/mL) resuspended in 1× PBS. Afterward, the electrodes were washed with 1× PBS (Au/MUA/EDC–NHS/PLL/EVs) and then blocked by incubating for 1 h with 1% BSA in 1× PBS (Au/MUA/EDC–NHS/PLL/EVs/BSA). Next, electrodes with captured EVs were incubated for 1 h in a 1:1 mixture of AuNPs/anti-CD63@Pb^{2+} and AuNPs/anti-CD81@Cu^{2+} at a 8.95×10^{10} particles/mL concentration washed thoroughly with DI water and then analyzed using SWV. The total assay time was defined as 4 h allowing for EV detection of each functionalized Au electrode.

For detection of podocin and nephrin, electrodes containing an anti-CD63 layer were incubated with EVs for 2 h. We used 120 μL of clinical urine after removing debris via centrifugation at 2000*g* for 10 min. Afterward, the electrodes were washed with 1× PBS (Au/MUA/EDC–NHS/CD63/BSA/EVs). Subsequently, a mixed solution containing AuNPs/anti-nephrin@Pb^{2+} and AuNPs/anti-podocin@Cu^{2+} was incubated on the electrodes with captured EVs for 1 h. Finally, the electrode surfaces were washed thoroughly with DI water and SWV was then used to detect redox peaks for Pb^{2+} and Cu^{2+} and infer the podocin to nephrin ratio of EVs. The total assay time was 3 h. To calculate the podocin to nephrin ratio, total charge (Q) was analyzed for each peak from SWV and then Q values were normalized according to the formula (normalized Q, $\bar{Q} = Q_{\text{EVs}} - Q_{\text{isotype control Abs}}$). The podocin/nephrin ratio was calculated by dividing $\bar{Q}$ of podocin to $\bar{Q}$ of nephrin.

Flow Cytometry Analysis of Urine Samples.

Urinary EVs were analyzed using a FACSCanto II flow cytometry system (BD Biosciences, San Jose, CA) as previously described.[9,62] Briefly, a total 10 μL of the sample was diluted with Hanks'/HEPES (HHBS)-buffered saline solution (pH 7.4) and then stained with 3 μL of podocin conjugated with fluorescein isothiocyanate (Bioss Antibodies Inc, USA) and nephrin (Biorbyt, Cambridge, UK) Abs conjugated with phycoerythrin. Corresponding IgG isotype controls obtained from the same companies were used to set up the thresholds. Following incubation at room temperature in the dark for 30 min, 800 μL of HHBS and 100 μL of TruCOUNT beads (BD Biosciences, San Jose, CA) were added and analyzed immediately. The count of all either nephrin- or podocin-positive EVs was calculated, considering the number of events registered in the corresponding quadrants (for nephrin, $Q_1 + Q_2$ and for podocin, $Q_2 + Q_4$), total number of gated TruCount beads (set up to 1500 for this experiment), count of beads added to the test tube (4655 in this case), dilution of the sample (100 for this sample), and total volume in the test tube (1000 μL). The following formula was used

$$\text{nephrin positive EVs} = (Q_1 + Q_2)/1500 \times 4655 \times 100/1000$$

$$\text{podocin positive EVs} = (Q_2 + Q_4)/1500 \times 4655 \times 100/1000$$

Isotype Abs were labeled and quantified in the same way as described above for podocin and nephrin where positive events with the isotype control were deemed background/noise and were subtracted from podocin and nephrin events. The counts of EVs were expressed as EVs/μL of the sample. The podocin/nephrin ratio was calculated by dividing podocin-positive to nephrin-positive EVs.

Supplementary Material

Refer to Web version on PubMed Central for supplementary material.

ACKNOWLEDGMENTS

This work was funded by grants from the NIH (GM123757, HD96993, and DK111378). We appreciate technical advice provided by Dr. Yong Duk Han for this study.

REFERENCES

(1). Kordasht HK; Hasanzadeh M. Biomedical Analysis of Exosomes Using Biosensing Methods: Recent Progress. Anal. Methods 2020, 12, 2795–2811. [PubMed: 32930202]

(2). Serrano-Pertierra E; Oliveira-Rodríguez M; Matos M; Gutiérrez G; Moyano A; Salvador M; Rivas M; Blanco-López MC Extracellular Vesicles: Current Analytical Techniques for Detection and Quantification. Biomolecules 2020, 10, 824. [PubMed: 32481493]

(3). Wang J; Huang X; Xie J; Han Y; Huang Y; Zhang H. Exosomal Analysis: Advances in Biosensor Technology. Clin. Chim. Acta 2021, 518, 142–150. [PubMed: 33811925]

(4). Campos-Silva C; Suárez H; Jara-Acevedo R; Linares-Espinós E; Martinez-Piñeiro L; Yáñez-Mó M; Valés-Gómez M. High Sensitivity Detection of Extracellular Vesicles Immune-Captured from Urine by Conventional Flow Cytometry. Sci. Rep 2019, 9, 2042. [PubMed: 30765839]

(5). Chiriacò M; Bianco M; Nigro A; Primiceri E; Ferrara F; Romano A; Quattrini A; Furlan R; Arima V; Maruccio G. Lab-on-Chip for Exosomes and Microvesicles Detection and Characterization. Sensors 2018, 18, 3175. [PubMed: 30241303]

(6). Yan H; Li Y; Cheng S; Zeng Y. Advances in Analytical Technologies for Extracellular Vesicles. Anal. Chem 2021, 93, 4739–4774. [PubMed: 33635060]

(7). Merchant ML; Rood IM; Deegens JKJ; Klein JB Isolation and Characterization of Urinary Extracellular Vesicles: Implications for Biomarker Discovery. Nat. Rev. Nephrol 2017, 13, 731–749. [PubMed: 29081510]

(8). Li J; Liu H; Mauer AS; Lucien F; Raiter A; Bandla H; Mounajjed T; Yin Z; Glaser KJ; Yin M; Malhi H. Characterization of Cellular Sources and Circulating Levels of Extracellular Vesicles in a Dietary Murine Model of Nonalcoholic Steatohepatitis. Hepatol. Commun 2019, 3, 1235–1249. [PubMed: 31497744]

(9). Gilani SI; Anderson UD; Jayachandran M; Weissgerber TL; Zand L; White WM; Milic N; Suarez MLG; Vallapureddy RR; Nääv Å; Erlandsson L; Lieske JC; Grande JP; Nath KA; Hansson SR; Garovic VD Urinary Extracellular Vesicles of Podocyte Origin and Renal Injury in Preeclampsia. J. Am. Soc. Nephrol 2017, 28, 3363–3372. [PubMed: 28729288]

(10). Zhou Q; Rahimian A; Son K; Shin D-S; Patel T; Revzin A. Development of an Aptasensor for Electrochemical Detection of Exosomes. Methods 2016, 97, 88–93. [PubMed: 26500145]

(11). Erdbrügger U; Le TH Extracellular Vesicles in Renal Diseases: More than Novel Biomarkers? J. Am. Soc. Nephrol 2016, 27, 12–26. [PubMed: 26251351]

(12). Karpman D; Ståhl A.-l.; Arvidsson I. Extracellular Vesicles in Renal Disease. Nat. Rev. Nephrol 2017, 13, 545–562. [PubMed: 28736435]

(13). Garovic VD; Wagner SJ; Petrovic LM; Gray CE; Hall P; Sugimoto H; Kalluri R; Grande JP Glomerular Expression of Nephrin and Synaptopodin, but not Podocin, is Decreased in Kidney Sections from Women with Preeclampsia. Nephrol. Dial. Transplant 2007, 22, 1136–1143. [PubMed: 17255128]

(14). Wang J; Ma P; Kim DH; Liu B-F; Demirci U. Towards Microfluidic-Based Exosome Isolation and Detection for Tumor Therapy. Nano Today 2021, 37, 101066.

(15). Singh K; Nalabotala R; Koo KM; Bose S; Nayak R; Shiddiky MJA Separation of Distinct Exosome Subpopulations: Isolation and Characterization Approaches and Their Associated Challenges. Analyst 2021, 146, 3731–3749. [PubMed: 33988193]

(16). Fan Y; Duan X; Zhao M; Wei X; Wu J; Chen W; Liu P; Cheng W; Cheng Q; Ding S. High-Sensitive and Multiplex Biosensing Assay of NSCLC-Derived Exosomes via Different Recognition Sites Based on SPRi Array. Biosens. Bioelectron 2020, 154, 112066.

(17). Liang K; Liu F; Fan J; Sun D; Liu C; Lyon CJ; Bernard DW; Li Y; Yokoi K; Katz MH; Koay EJ; Zhao Z; Hu Y. Nanoplasmonic Quantification of Tumour-Derived Extracellular Vesicles in Plasma Microsamples for Diagnosis and Treatment Monitoring. Nat. Biomed. Eng 2017, 1, 0021. [PubMed: 28791195]

(18). Sina AAI; Vaidyanathan R; Dey S; Carrascosa LG; Shiddiky MJA; Trau M. Real Time and Label Free Profiling of Clinically Relevant Exosomes. Sci. Rep 2016, 6, 30460. [PubMed: 27464736]

(19). Boriachek K; Islam MN; Gopalan V; Lam AK; Nguyen N-T; Shiddiky MJA Quantum Dot-Based Sensitive Detection of Disease Specific Exosome in Serum. Analyst 2017, 142, 2211–2219. [PubMed: 28534915]

(20). Jeong S; Park J; Pathania D; Castro CM; Weissleder R; Lee H. Integrated Magneto–Electrochemical Sensor for Exosome Analysis. ACS Nano 2016, 10, 1802–1809. [PubMed: 26808216]

(21). Farhana FZ; Umer M; Saeed A; Pannu AS; Shahbazi M; Jabur A; Nam HJ; Ostrikov K; Sonar P; Firoz SH; Shiddiky MJA Isolation and Detection of Exosomes Using Fe_2O_3 Nanoparticles. ACS Appl. Nano Mater. 2021, 4, 1175–1186.

(22). Boriachek K; Masud MK; Palma C; Phan H-P; Yamauchi Y; Hossain MSA; Nguyen N-T; Salomon C; Shiddiky MJA Avoiding Pre-Isolation Step in Exosome Analysis: Direct Isolation and Sensitive Detection of Exosomes Using Gold-Loaded Nanoporous Ferric Oxide Nanozymes. Anal. Chem 2019, 91, 3827–3834. [PubMed: 30735354]

(23). Park J; Park JS; Huang C-H; Jo A; Cook K; Wang R; Lin H-Y; Van Deun J; Li H; Min J; Wang L; Yoon G; Carter BS; Balaj L; Choi G-S; Castro CM; Weissleder R; Lee H. An Integrated Magneto-Electrochemical Device for the Rapid Profiling of Tumour Extracellular Vesicles from Blood Plasma. Nat. Biomed. Eng 2021, 5, 678–689. [PubMed: 34183802]

(24). Cao Y; Li L; Han B; Wang Y; Dai Y; Zhao J. A Catalytic Molecule Machine-Driven Biosensing Method for Amplified Electrochemical Detection of Exosomes. Biosens. Bioelectron 2019, 141, 111397.

(25). Zhang L; Gu C; Wen J; Liu G; Liu H; Li L. Recent Advances in Nanomaterial-Based Biosensors for the Detection of Exosomes. Anal. Bioanal. Chem 2021, 413, 83–102. [PubMed: 33164151]

(26). Xu L; Shoaie N; Jahanpeyma F; Zhao J; Azimzadeh M; Al-Jamal KT Optical, Electrochemical and Electrical (Nano) Biosensors for Detection of Exosomes: A Comprehensive Overview. Biosens. Bioelectron 2020, 161, 112222.

(27). Xu H; Liao C; Zuo P; Liu Z; Ye B-C Magnetic-Based Microfluidic Device for On-Chip Isolation and Detection of Tumor-Derived Exosomes. Anal. Chem 2018, 90, 13451–13458. [PubMed: 30234974]

(28). Wang Z; Liu N; Ma Z. Platinum Porous Nanoparticles Hybrid with Metal Ions as Probes for Simultaneous Detection of Multiplex Cancer Biomarkers. Biosens. Bioelectron 2014, 53, 324–329. [PubMed: 24176967]

(29). Xu T; Jia X; Chen X; Ma Z. Simultaneous Electrochemical Detection of Multiple Tumor Markers Using Metal Ions Tagged Immunocolloidal Gold. Biosens. Bioelectron 2014, 56, 174–179. [PubMed: 24487105]

(30). Feng L-N; Bian Z-P; Peng J; Jiang F; Yang G-H; Zhu Y-D; Yang D; Jiang L-P; Zhu J-J Ultrasensitive Multianalyte Electrochemical Immunoassay Based on Metal Ion Functionalized Titanium Phosphate Nanospheres. Anal. Chem 2012, 84, 7810–7815. [PubMed: 22913388]

(31). Wang J; Liu G; Merkoçi A. Electrochemical Coding Technology for Simultaneous Detection of Multiple DNA Targets. J. Am. Chem. Soc 2003, 125, 3214–3215. [PubMed: 12630867]

(32). Zhang W; Besford QA; Christofferson AJ; Charchar P; Richardson JJ; Elbourne A; Kempe K; Hagemeyer CE; Field MR; McConville CF; Yarovsky I; Caruso F. Cobalt-Directed Assembly of Antibodies onto Metal–Phenolic Networks for Enhanced Particle Targeting. Nano Lett. 2020, 20, 2660–2666. [PubMed: 32155075]

(33). Kumar A; Wahlund P-O; Kepka C; Galaev IY; Mattiasson B. Purification of Histidine-Tagged Single-Chain Fv-Antibody Fragments by Metal Chelate Affinity Precipitation Using Thermoresponsive Copolymers. Biotechnol. Bioeng 2003, 84, 494–503. [PubMed: 14574708]

(34). Zhang C; Su J; Zhu H; Xiong J; Liu X; Li D; Chen Y; Li Y. The Removal of Heavy Metal Ions from Aqueous Solutions by Amine Functionalized Cellulose Pretreated with Microwave-H_2O_2. RSC Adv. 2017, 7, 34182–34191.

(35). Wang Y; Wang L; Zhang J; Wang G; Chen W; Chen L; Zhang X. Preparation of Colloidal Gold Immunochromatographic Strip for Detection of Paragonimiasis Skrjabini. PLoS One 2014, 9, No. e92034.

(36). Kulabhusan PK; Rajwade JM; Sugumar V; Taju G; Sahul Hameed AS; Paknikar KM Field-Useable Lateral Flow Immunoassay for the Rapid Detection of White Spot Syndrome Virus (WSSV). PLoS One 2017, 12, No. e0169012.

(37). Verkhoturov DS; Crulhas BP; Eller MJ; Han YD; Verkhoturov SV; Bisrat Y; Revzin A; Schweikert EA Nanoprojectile Secondary Ion Mass Spectrometry for Analysis of Extracellular Vesicles. Anal. Chem 2021, 93, 7481–7490. [PubMed: 33988360]

(38). Majumder M; Rendall CS; Eukel JA; Wang JYL; Behabtu N; Pint CL; Liu T-Y; Orbaek AW; Mirri F; Nam J; Barron AR; Hauge RH; Schmidt HK; Pasquali M. Overcoming the “Coffee-Stain” Effect by Compositional Marangoni-Flow-Assisted Drop-Drying. J. Phys. Chem. B 2012, 116, 6536–6542. [PubMed: 22587569]

(39). Tsai Y-C; Li S-C; Chen J-M Cast Thin Film Biosensor Design Based on a Nafion Backbone, a Multiwalled Carbon Nanotube Conduit, and a Glucose Oxidase Function. Langmuir 2005, 21, 3653–3658. [PubMed: 15807616]

(40). Lu J; Drzal LT; Worden RM; Lee I. Simple Fabrication of a Highly Sensitive Glucose Biosensor Using Enzymes Immobilized in Exfoliated Graphite Nanoplatelets Nafion Membrane. Chem. Mater 2007, 19, 6240–6246.

(41). Wang Z; Gong L; Zeng H; Yang T; Luo X. A Novel Ratiometric Electrochemical Cupric Ion Sensing Strategy Based on Unmodified Electrode. Anal. Chim. Acta 2021, 1146, 11–16. [PubMed: 33461705]

(42). Lin M; Cho M; Choe W-S; Son Y; Lee Y. Electrochemical Detection of Copper Ion Using a Modified Copolythiophene Electrode. Electrochim. Acta 2009, 54, 7012–7017.

(43). Chow E; Hibbert DB; Gooding JJ Electrochemical Detection of Lead Ions via the Covalent Attachment of Human Angiotensin I to Mercaptopropionic Acid and Thioctic Acid Self-Assembled Monolayers. Anal. Chim. Acta 2005, 543, 167–176.

(44). Lin M; Cho M; Choe W-S; Lee Y. Electrochemical Detection of Lead Ion Based on a Peptide Modified Electrode. Electroanalysis 2016, 28, 998–1002.

(45). Zhang H; Qiao B; Guo Q; Jiang J; Cai C; Shen J. A Facile and Label-Free Electrochemical Aptasensor for Tumour-Derived Extracellular Vesicle Detection Based on the Target-Induced Proximity Hybridization of Split Aptamers. Analyst 2020, 145, 3557–3563. [PubMed: 32309839]

(46). Kuralay F; Dükar N; Bayramlı Y. Poly-L-lysine Coated Surfaces for Ultrasensitive Nucleic Acid Detection. Electroanalysis 2018, 30, 1556–1565. [PubMed: 32313411]

(47). Zhang D; Zhang Y; Zheng L; Zhan Y; He L. Graphene Oxide/Poly-L-Lysine Assembled Layer for Adhesion and Electrochemical Impedance Detection of Leukemia K562 Cancer Cells. Biosens. Bioelectron 2013, 42, 112–118. [PubMed: 23202339]

(48). Haji-Hashemi H; Norouzi P; Safarnejad MR; Ganjali MR Label-Free Electrochemical Immunosensor for Direct Detection of Citrus Tristeza Virus Using Modified Gold Electrode. Sens. Actuators, B 2017, 244, 211–216.

(49). Ding S-J; Chang B-W; Wu C-C; Lai M-F; Chang H-C Electrochemical Evaluation of Avidin–Biotin Interaction on Self-Assembled Gold Electrodes. Electrochim. Acta 2005, 50, 3660–3666.

(50). Xia Y; Liu M; Wang L; Yan A; He W; Chen M; Lan J; Xu J; Guan L; Chen J. A Visible and Colorimetric Aptasensor Based on DNA-Capped Single-Walled Carbon Nanotubes for Detection of Exosomes. Biosens. Bioelectron 2017, 92, 8–15. [PubMed: 28167415]

(51). Kilic T; Valinhas ATDS; Wall I; Renaud P; Carrara S. Label-Free Detection of Hypoxia-Induced Extracellular Vesicle Secretion from MCF-7 Cells. Sci. Rep 2018, 8, 9402. [PubMed: 29925885]

(52). Im H; Shao H; Park YI; Peterson VM; Castro CM; Weissleder R; Lee H. Label-Free Detection and Molecular Profiling of Exosomes with a Nano-Plasmonic Sensor. Nat. Biotechnol 2014, 32, 490–495. [PubMed: 24752081]

(53). Shao H; Chung J; Balaj L; Charest A; Bigner DD; Carter BS; Hochberg FH; Breakefield XO; Weissleder R; Lee H. Protein Typing of Circulating Microvesicles Allows Real-Time Monitoring of Glioblastoma Therapy. Nat. Med 2012, 18, 1835. [PubMed: 23142818]

(54). Xu R; Greening DW; Zhu H-J; Takahashi N; Simpson RJ Extracellular Vesicle Isolation and Characterization: Toward Clinical Application. J. Clin. Invest 2016, 126, 1152–1162. [PubMed: 27035807]

(55). Coumans FAW; Gool EL; Nieuwland R. Bulk Immunoassays for Analysis of Extracellular Vesicles. Platelets 2017, 28, 242–248. [PubMed: 28102735]

(56). Wang Y; Liu Z; Wang X; Dai Y; Li X; Gao S; Yu P; Lin Q; Fan Z; Ping Y; Wang D; Lin X; Zheng Z; Liu W; Tao Z. Rapid and Quantitative Analysis of Exosomes by a Chemiluminescence Immunoassay Using Superparamagnetic Iron Oxide Particles. J. Biomed. Nanotechnol 2019, 15, 1792–1800. [PubMed: 31219017]

(57). He F; Wang J; Yin B-C; Ye B-C Quantification of Exosome Based on a Copper-Mediated Signal Amplification Strategy. Anal. Chem 2018, 90, 8072–8079. [PubMed: 29890831]

(58). He D; Ho S-L; Chan H-N; Wang H; Hai L; He X; Wang K; Li H-W Molecular-Recognition-Based DNA Nanodevices for Enhancing the Direct Visualization and Quantification of Single Vesicles of Tumor Exosomes in Plasma Microsamples. Anal. Chem 2019, 91, 2768–2775. [PubMed: 30644724]

(59). He F; Liu H; Guo X; Yin B-C; Ye B-C Direct Exosome Quantification via Bivalent-Cholesterol-Labeled DNA Anchor for Signal Amplification. Anal. Chem 2017, 89, 12968–12975. [PubMed: 29139297]

(60). Eller MJ; Verkhoturov SV; Schweikert EA Testing Molecular Homogeneity at the Nanoscale with Massive Cluster Secondary Ion Mass Spectrometry. Anal. Chem 2016, 88, 7639–7646. [PubMed: 27373342]

(61). Rickman RD; Verkhoturov SV; Hager GJ; Schweikert EA; Bennett JA Multiple Secondary Ion Emission from keV Massive Gold Projectile Impacts. Int. J. Mass Spectrom. 2005, 241, 57–61.

(62). Jayachandran M; Lugo G; Heiling H; Miller VM; Rule AD; Lieske JC Extracellular Vesicles in Urine of Women with but not Without Kidney Stones Manifest Patterns Similar to Men: A Case Control Study. Biol. Sex Differ. 2015, 6, 2. [PubMed: 25729563]

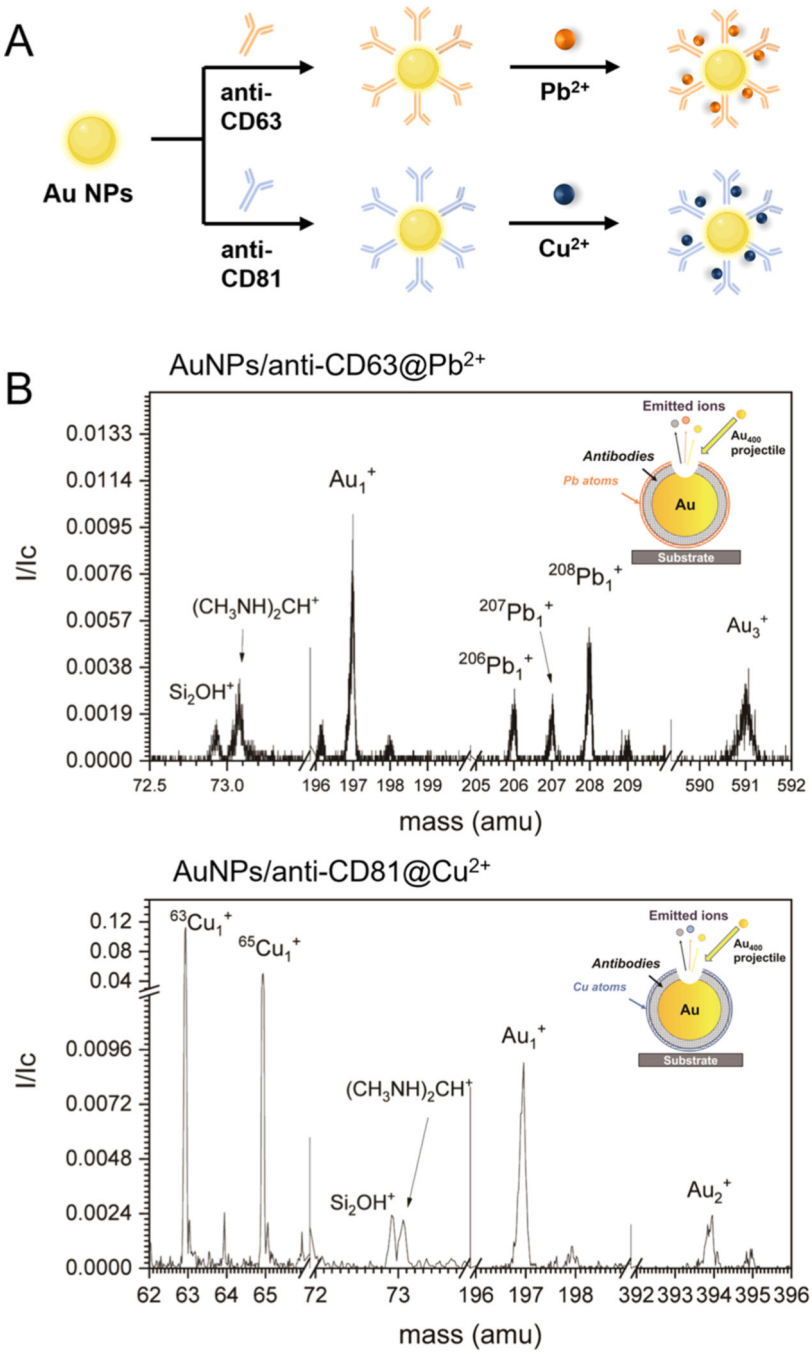

Scheme 1. Working Principle of the Nanoparticle-Enabled Electrochemical Immunoassay for Detection of EV Surface Markers. Electrode Surfaces Were Washed after EV Capture and Immunoprobe Labeling Steps[a]

[a]BSA blocking was used to minimize non-specific interactions. Immunoprobes were functionalized with the isotype control Abs to assess off-target binding effects.

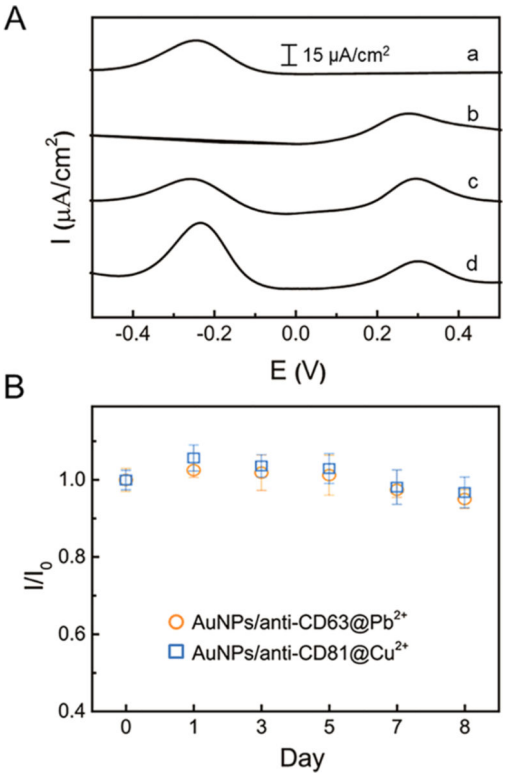

Figure 1.

Preparation and characterization of immunoprobes. (A) Steps required for functionalization of AuNPs. Attachment of Abs occurs via EDC–NHS bonding. Metal ions interact with Abs by coordination bonding. (B) NP-SIMS analysis of immunoprobes AuNPs/anti-CD63@Pb^{2+} (top) and AuNPs/anti-CD63@Cu^{2+} (bottom). Impacts were selected based on detection of Au_2^+ or Au_3^+, characteristic of the immunogold particles. The Y-axis represents the measured intensity divided by the number of measurements in each experiment. Selected regions of the mass spectra are shown highlighting secondary-ion characteristic to the Abs, silicon support, gold particles, and metal ions.

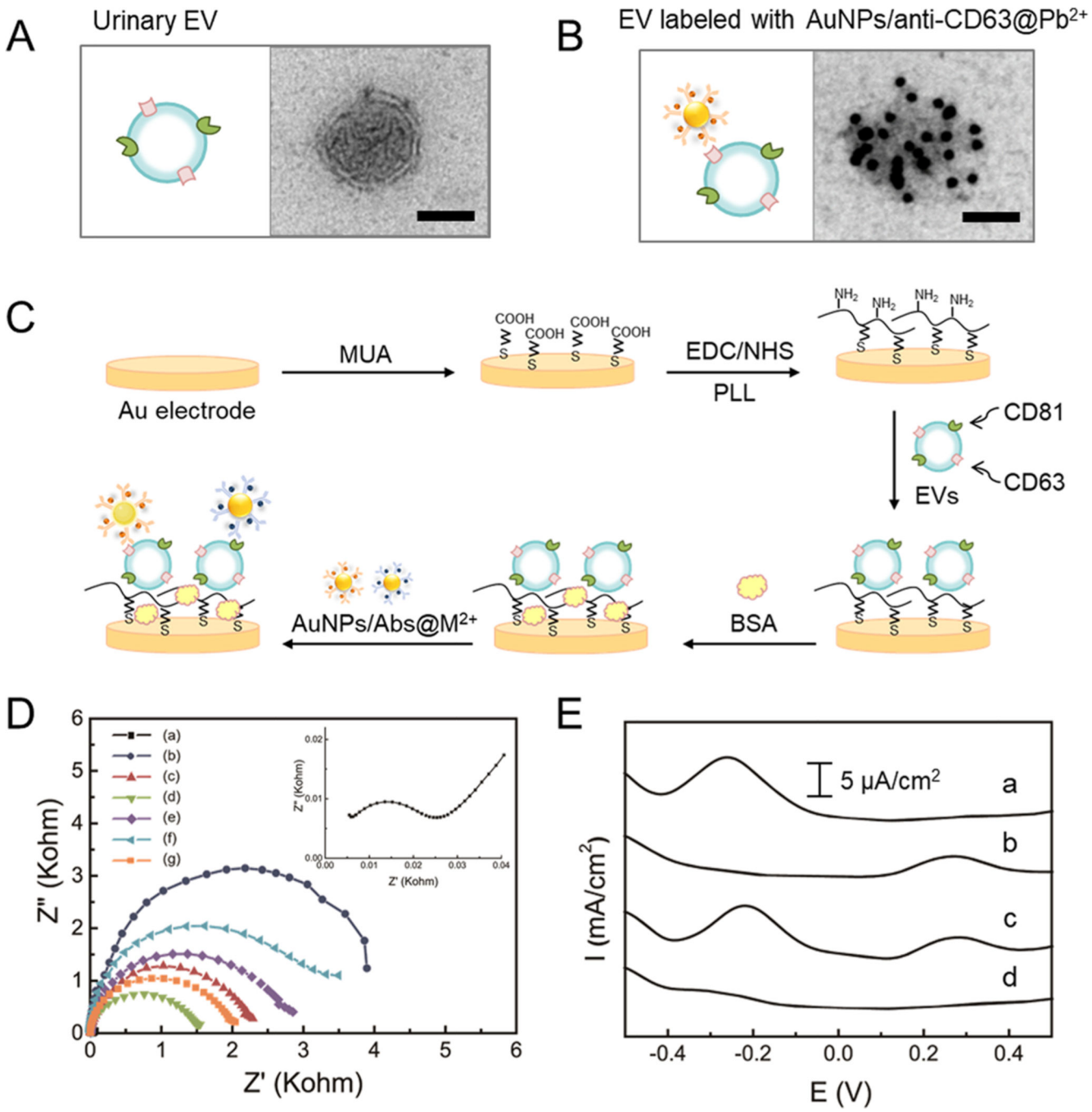

Figure 2.

Electrochemical characterization of immunoprobes. (A) SWV response of different ratios of AuNPs/anti-CD63@Pb^{2+} to AuNPs/anti-CD81@Cu^{2+}; (a) 1:0, (b) 0:1, (c) 1:1, and (d) 2:1. (B) Stability of AuNPs/Ab@M^{2+} immunoprobes when stored at 4 °C in HEPES buffer for 8 days. Peak current from SWV measurement on a given day (I) was divided by the value of the peak current immediately after electrode preparation (I_0).

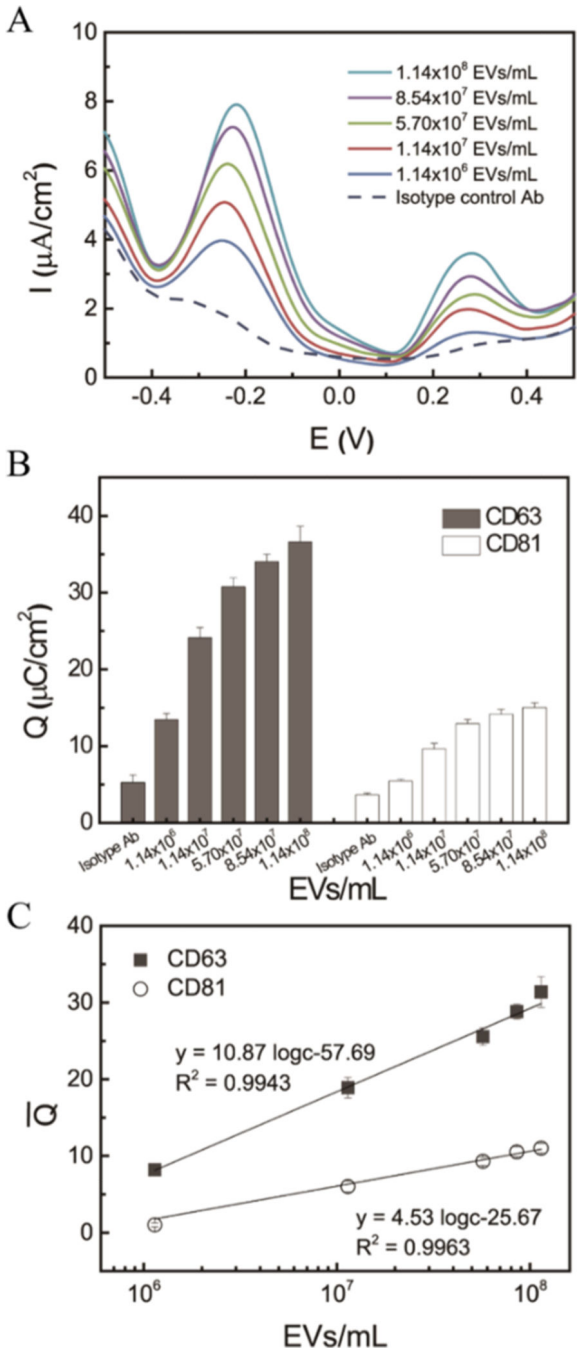

Figure 3.

Construction of electrodes and detection of EVs. (A,B) Representative TEM images of EVs before (A) and after (B) incubation with immunoprobes. Scale bar, 100 nm. (C) Process flow for electrode modification and EV capture. (D) Characterization of individual steps in the electrode functionalization and EV capture using EIS: (a) Au electrode (insert), (b) Au/MUA, (c) Au/MUA/EDC–NHS, (d) Au/MUA/EDC–NHS/PLL, (e) Au/MUA/EDC–NHS/PLL/EVs, (f) Au/MUA/EDC–NHS/PLL/EVs/BSA, and (g) Au/MUA/EDC–NHS/PLL/EVs/BSA/AuNPs–anti-CD63@Pb^{2+}. (E) Electrochemical (SWV) signals

from EV-containing electrodes that were incubated with immunoprobes specific to CD63 (a), CD81 (b), a 1:1 mixture of both types of immunoprobes (c), and electrode without EVs after incubating with a 1:1 mixture of both types of immunoprobes (d).

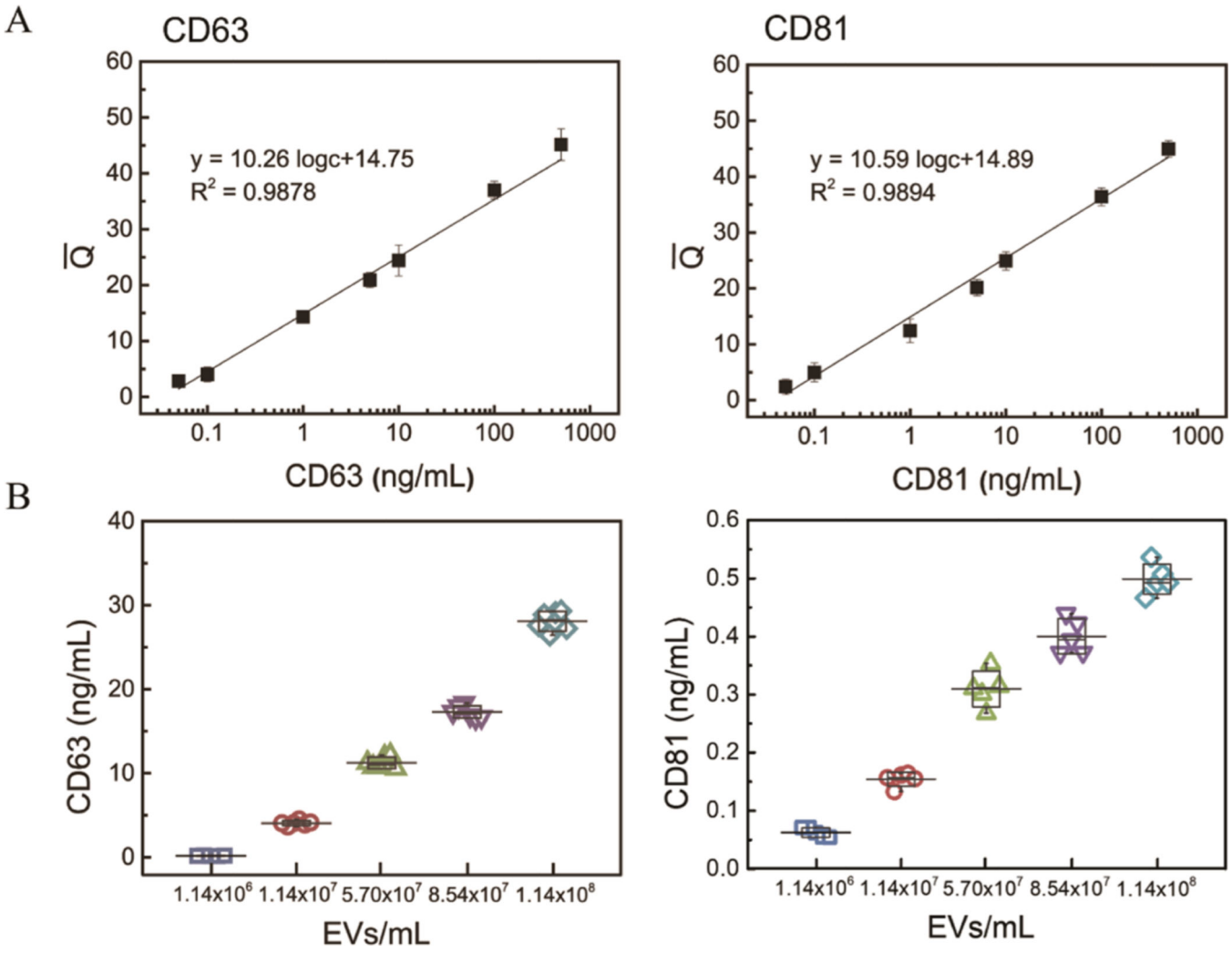

Figure 4.

Establishing detection limit and dynamic range for nanoparticle-enabled electrochemical immunoassay. (A) Electrochemical (SWV) analysis of electrodes containing different numbers of EVs after incubation with a mixture of AuNPs/anti-CD63@Pb^{2+} and AuNPs/anti-CD81@Cu^{2+} immunoprobes. (B) Total charge (Q) associated with each EV concentration. (C) Calibration curves of normalized charge $\overline{Q}$ vs EV concentration for CD63 and CD81 constructed for an EV concentration range of 1.14×10^6–1.14×10^8 particles/mL. Here, $\overline{Q} = Q_{\text{EVs}} - Q_{\text{isotype control Abs}}$ for detection of CD63 and CD81. The error bars represent the standard deviations from five different sensing electrodes ($n = 5$).

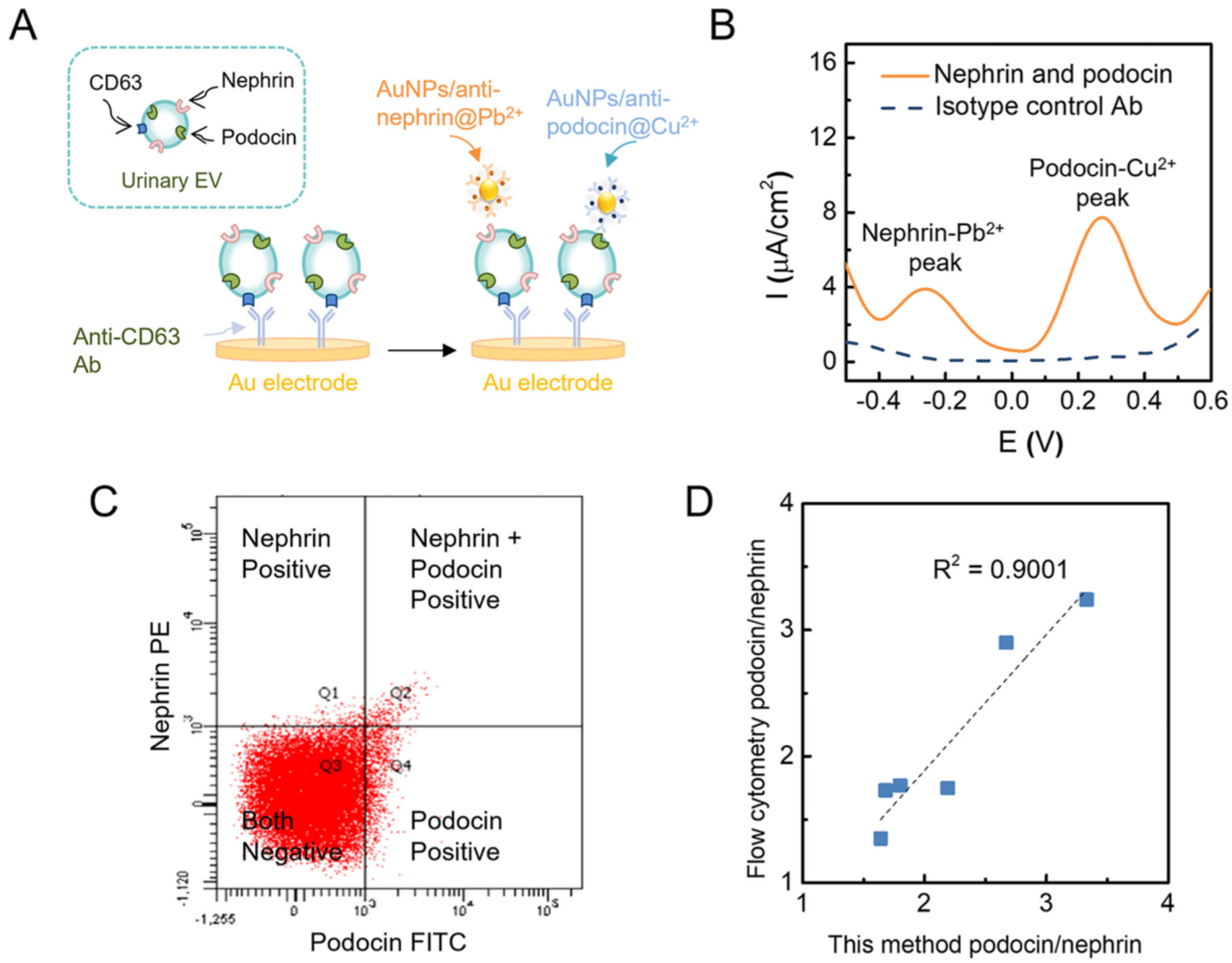

Figure 5.

Quantifying CD63 and CD81 expression on EVs. (A) Calibration curves obtained after immobilizing different concentrations of human recombinant CD63 and CD81 proteins on the electrode surfaces. The linear plot of the normalized total charge ($\bar{Q} = Q - Q_0$) changes as a function of the logarithm of the concentration of recombinant CD63 or CD81 (0–500 ng/mL). The error bars represent the standard deviations from three different sensing electrodes ($n = 3$). (B) Plots correlating concentration of CD63 or CD81 to the concentration of EVs allow to quantify surface marker expression. Values for normalized total charge $\bar{Q}$ associated with immobilization of recombinant proteins were correlated with EV concentration using calibration curves from Figure 4C to construct plots presented here. The data points and error bars represent average and standard deviations of measurements from five different electrodes containing captured EVs ($n = 5$).

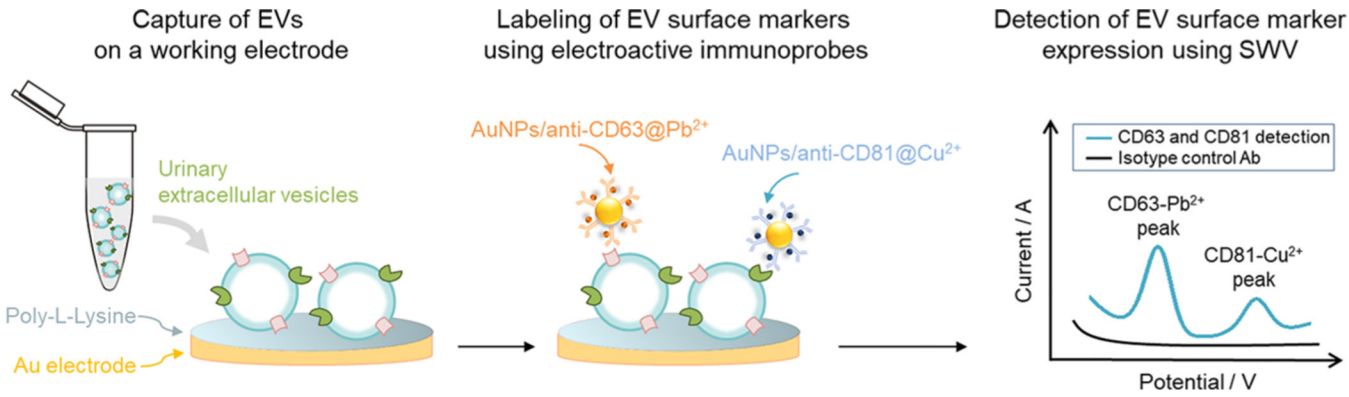

Figure 6.

Using clinical samples to validate electrochemical immunoassay against flow cytometry. (A) Principle of assay operation. Electrodes were functionalized with anti-CD63 for capture of EVs. Immunoprobes targeting nephrin and podocin on urinary EVs were then used for labeling and electrochemical detection. (B) Representative electrochemical (SWV) analysis of EVs from a clinical sample captured on a working electrode. AuNPs/anti-nephrin@Pb^{2+} and AuNPs/anti-podocin@Cu^{2+} immunoprobes were used to label EVs and generate dual redox peaks. No redox activity was observed when electrodes containing EVs were labeled with isotype control immunoprobes (dashed line). (C) Representative flow cytometry analysis of nephrin and podocin expression in clinical EVs. The same sample was characterized by flow cytometry and electrochemical analysis. (D) plot of podocin/nephrin ratios obtained with electrochemical immunoassay (this method) and flow cytometry based on urine samples from six pregnant women ($n = 6$). The results showed high correlation ($R^2 = 0.9001$) between our method and flow cytometry.